Archival Report

Biological Psychiatry

Astrocytic Contributions to Synaptic and Learning Abnormalities in a Mouse Model of Fragile X Syndrome

Jennifer L. Hodges, Xinzhu Yu, Anthony Gilmore, Hannah Bennett, Michelle Tjia, James F. Perna, Chia-Chien Chen, Xiang Li, Ju Lu, and Yi Zuo

ABSTRACT

BACKGROUND: Fragile X syndrome (FXS) is the most common type of mental retardation attributable to a single-gene mutation. It is caused by *FMR1* gene silencing and the consequent loss of its protein product, fragile X mental retardation protein. *Fmr1* global knockout (KO) mice recapitulate many behavioral and synaptic phenotypes associated with FXS. Abundant evidence suggests that astrocytes are important contributors to neurological diseases. This study investigates astrocytic contributions to the progression of synaptic abnormalities and learning impairments associated with FXS.

METHODS: Taking advantage of the Cre-lox system, we generated and characterized mice in which fragile X mental retardation protein is selectively deleted or exclusively expressed in astrocytes. We performed in vivo two-photon imaging to track spine dynamics/morphology along dendrites of neurons in the motor cortex and examined associated behavioral defects.

RESULTS: We found that adult astrocyte-specific *Fmr1* KO mice displayed increased spine density in the motor cortex and impaired motor-skill learning. The learning defect coincided with a lack of enhanced spine dynamics in the motor cortex that normally occurs in response to motor skill acquisition. Although spine density was normal at 1 month of age in astrocyte-specific *Fmr1* KO mice, new spines formed at an elevated rate. Furthermore, fragile X mental retardation protein expression in only astrocytes was insufficient to rescue most spine or behavioral defects.

CONCLUSIONS: Our work suggests a joint astrocytic-neuronal contribution to FXS pathogenesis and reveals that heightened spine formation during adolescence precedes the overabundance of spines and behavioral defects found in adult *Fmr1* KO mice.

Keywords: Astrocytes, Dendritic spines, Fragile X syndrome, *Fmr1*, Motor cortex, Motor learning

http://dx.doi.org/10.1016/j.biopsych.2016.08.036

Fragile X syndrome (FXS) is the most frequent form of inherited mental retardation, affecting approximately 1 in 4000 males and 1 in 6000 females of all races and ethnic groups (1). Patients with FXS display a wide spectrum of phenotypes, including moderate to severe mental retardation, autistic behavior, macroorchidism, predisposition to epileptic seizures, and facial abnormalities (2–4). They also experience huge social challenges, placing a great economic and emotional burden on their families. Nearly all FXS cases are caused by a trinucleotide repeat expansion in the X-linked *FMR1* gene, which silences its transcription and abolishes the expression of its protein product, fragile X mental retardation protein (FMRP) (5). FMRP regulates the transportation and translation of messenger RNAs (mRNAs) that are important for dendritic growth, synapse development, and plasticity (6).

Spine morphology and density are paramount to synaptic function and connectivity (7,8). In vivo imaging studies on global *Fmr1* knockout (KO) mice reveal elevated spine dynamics along apical dendrites of layer II/III and layer V pyramidal neurons in motor and barrel cortices at various ages, suggesting that the absence of FMRP reduces the stability of synapses (9–11). Furthermore, in both patients with FXS (12) and adult global *Fmr1* KO mice (13,14), the density of long and thin spines on apical dendrites of cortical pyramidal neurons is abnormally high, reminiscent of the abundance of immature spines found during early development (15). Thus, it has been hypothesized that the absence of FMRP causes abnormalities in spine development, which in turn alter synaptic connectivity and ultimately result in behavioral impairments, including learning defects (14).

The aforementioned spine phenotypes have elicited copious research on the neuronal mechanisms of FXS (16). However, little is known regarding the contribution of non-neuronal cells in the brain, for example, glia, to FXS pathogenesis. As the most abundant glial cells in the mammalian brain, astrocytes modulate synaptic structure and function and are implicated in many neurodevelopmental diseases (17). Although FMRP expression among individual cell types in

SEE COMMENTARY ON PAGE e11

ISSN: 0006-3223

the human brain has not been examined, FMRP has been found in astrocytes of the mouse brain (18–20), which suggests a possible astrocytic role in FXS pathogenesis. In support of this notion, culturing wild-type neurons with *Fmr1*-deficient astrocytes leads to the development of abnormal dendritic morphologies, reduces synaptic protein clusters, and increases levels of extracellular glutamate (19,21). These studies provide evidence that astrocytic FMRP is vital to the development of neurons and synapses in vitro. However, the contribution of astrocytes to the progression of dendritic spine and behavioral defects in FXS in vivo remains elusive.

METHODS AND MATERIALS

Experimental Animals

The Institutional Animal Care and Use Committee of University of California Santa Cruz approved all animal care and experimental procedures. The *Fmr1*^{fl} and *Fmr1*^{neo} mice were obtained from Dr. David L. Nelson, Baylor College of Medicine; the global *Fmr1* KO mice, from Dr. Stephen T. Warren, Emory University; the *mGFAP-Cre*$^{+}$ mice (line 73.12), from Dr. Michael V. Sofroniew, University of California, Los Angeles; and the *S100β-GFP* mice, from Dr. Wesley J. Thompson, Texas A&M University. *Thy1*-YFP-H and *Rosa26*^{tdTomato} mice were purchased from Jackson Laboratory (Bar Harbor, ME). All mice were backcrossed with C57BL/6 mice more than 10 generations to produce congenic strains. Male mice were used in all experiments.

Cortical Astrocyte Culture and Immunocytochemistry

The protocol to prepare primary astrocyte cultures has been previously described (22). Detailed procedures of culture preparation and immunocytochemistry are described in the Supplemental Methods.

Immunohistochemistry for Cortical Sections

Mice were transcardially perfused with 4% paraformaldehyde fixative in 0.1 mol/L phosphate-buffered saline (PBS). Brains were postfixed in 4% paraformaldehyde fixative/PBS overnight at 4°C and cryoprotected in 30% sucrose. For most experiments, 40-μm brain sections were used. Sections were permeabilized and blocked with 0.5% Triton X-100 and 10% normal goat serum/PBS, then incubated with the following primary antibodies in 0.5% Triton X-100/PBS at 4°C overnight: rabbit anti-S100β (1:1000; Cat. no. Z0311; DakoCytomation, Carpinteria, CA), mouse anti-NeuN (1:2000; Cat. no. MAB377; Millipore, Darmstadt, Germany), rabbit anti-Olig2 (1:500; Cat. no. AB9610; Millipore), goat anti-Iba1 (1:100; Cat. no. ab5076; Abcam, Cambridge, United Kingdom), or rabbit anti–glial fibrillary acidic protein (GFAP) (1:500; Cat. no. Z0334; DakoCytomation). For FMRP colabeling, 25-μm sections were incubated in 10 mmol/L sodium citrate (pH 6.0) with 0.05% Tween-20 at 85°C for 20 minutes, followed by 30 minutes in blocking solution (0.01% Triton X-100, 5% goat serum, 1% bovine serum albumin) at room temperature. Sections were labeled with mouse anti-FMRP 2F5-1 (1:1; Developmental Studies Hybridoma Bank, Iowa City, IA) and rabbit anti-NeuN (1:500; Cell Signaling Technology, Danvers, MA) at 4°C overnight. Sections were then incubated with Alexa Fluor 488- and 594-conjugated secondary antibodies (1:1000; Life Technologies, Carlsbad, CA) in 10% normal goat serum/PBS for 2 hours at room temperature for fluorescence imaging or with biotinylated secondary antibody (1:400; Vector Laboratories, Burlingame, CA), avidin-biotin complex (Vector Laboratories), and diaminobenzidine (Vector Laboratories) for bright-field imaging. Sections were mounted with Fluoromount-G mounting medium (Southern Biotechnology Associates, Inc., Birmingham, AL) or Vectashield hardening mounting medium (Vector Laboratories).

Western Blot

Cortical tissues were dissected from adult mice and homogenized in ice-cold radioimmunoprecipitation assay lysis buffer containing protease inhibitors (Roche, Basel, Switzerland). Nuclei were pelleted by centrifugation at 15,000 rpm, 4°C, for 15 minutes, and the supernatant was denatured in 2X Laemmli buffer. Cultured astrocytes were directly lysed and denatured in hot 2X Laemmli buffer. Denatured lysates were electrophoretically separated by a sodium dodecyl sulfate polyacrylamide gel electrophoresis gel and transferred onto a polyvinylidene difluoride membrane (Bio-Rad Laboratories, Hercules, CA). The following primary antibodies were used at 4°C overnight: mouse anti-FMRP 2F5-1 (1:1; Developmental Studies Hybridoma Bank), mouse anti-tubulin (1:5000; Cat. no. 8328; Sigma-Aldrich, St. Louis, MO), and rabbit anti-actin (1:1000; Cat. no. A2066; Sigma-Aldrich). Horse radish peroxidase–conjugated secondary antibody (anti-mouse immunoglobulin G or anti-rabbit immunoglobulin G; 1:5000; Cell Signaling Technology) was used for detection. All images shown are representative of at least three replications.

Fluorescence-Activated Cell Sorting Purification of Astrocytes and Quantitative Reverse-Transcriptase Polymerase Chain Reaction

Acute isolation of astrocytes from postnatal day 30 to 50 (P30–50) mice by immunopanning and fluorescence-activated cell sorting was adapted from previously established protocols (23,24). RNA was extracted from sorted astrocytes and prepped for reverse-transcriptase polymerase chain reaction. Details on the procedures are described in the Supplemental Methods.

Optical Imaging and Image Analysis for Brain Sections and Cultured Cells

Bright-field images were collected on a Zeiss Axio Imager.M2 microscope with either a 20X/NA 0.8 objective or a 40X/NA 1.4 oil-immersion objective, using the AxioVision software (Zeiss, Oberkochen, Germany). Confocal images were acquired on a Leica SP5 confocal system with either a 20X/NA 0.75 objective or a 63X/NA 1.4 oil-immersion objective (Leica, Wetzlar, Germany). Imaging settings were identical between samples in which fluorescence intensity was analyzed. Astrocyte number and morphology were analyzed from bright-field images using Stereo Investigator (MBF Bioscience, Williston, VT). Confocal images were used to analyze tdTomato-positive cells colabeled with various cell-specific markers by manual counting in

ImageJ. Custom-written scripts in MATLAB (The MathWorks, Inc., Natick, MA) were used to analyze the integrated density of FMRP fluorescent signal within NeuN-labeled cells from confocal images. One-way analysis of variance (ANOVA) and two-sided Student *t* test were used for statistical analyses. Data presented as mean ± SEM.

In Vivo Transcranial Imaging and Spine Data Analysis

Transcranial two-photon imaging and data analysis were performed as described previously (25,26). The number of mice used in each experiment is indicated in the figures and Supplemental Tables S1 and S2. All images were analyzed using ImageJ (National Institutes of Health, Bethesda, MD). Percentage of spines eliminated/formed was calculated as the number of spines eliminated/formed over the total spines counted in first-time images. Spine density was calculated by dividing spine numbers with dendritic length. Spines were classified into four categories—mushroom, stubby, thin, and other spines—based on their lengths and head diameters using previously published criteria (27). A spine is classified as a mushroom spine if the width of spine head $w_h > 2w_n$ (the width of spine neck); as a stubby spine if the length of spine $l < 0.5$ μm without spine neck; and as a thin spine if $l > 0.5$ μm and $w_h < 2w_n$. Spines with irregular morphology or pointing toward/away from the imaging plane are classified as others. Spine head diameter and spine neck length analysis were conducted as previously described (28,29). One-way ANOVA was performed for spine dynamic and spine density analyses, whereas two-way repeated-measures ANOVA was used for spine category analysis. Both were followed with Holm-Sidak post hoc multiple comparisons test. Data are presented as mean ± SD. Kolmogorov-Smirnov test was used to compare spine head diameter and spine neck length.

The Single-Pellet Reaching Task

We followed the previously described single-pellet reaching task protocol (25,30). The detailed procedure is described in the Supplemental Methods. Two-way ANOVA followed by Holm-Sidak post hoc multiple comparisons test was used to analyze the animal's reaching successes. Data are presented as mean ± SEM.

RESULTS

Generation and Characterization of Astrocyte-Specific *Fmr1* KO Mice

To explore astrocytic contributions to the neuropathology of FXS, we selectively deleted the *Fmr1* gene in astrocytes using a Cre-*loxP* recombination system. Because the mouse astrocytic GFAP promoter (*mGFAP-Cre*) has been shown to drive Cre expression postnatally in astrocytes (31–33), we crossed *mGFAP-Cre* mice with mice containing a floxed *Fmr1* gene (*Fmr1*^{fl}) (34). The male progeny inheriting both alleles are referred to as *Fmr1*$^{fl/y}$*;mGFAP-Cre*$^{+}$, or astrocyte-specific *Fmr1* KO mice. To determine the efficiency and specificity of mGFAP-Cre–mediated recombination, we also crossed *mGFAP-Cre* mice with a tdTomato reporter mouse line (*R26*^{tdTomato}) and characterized the tdTomato-positive cells in the cerebral cortex (Figure 1A–C). In the motor cortex, we found that in the superficial layers of the cortex encompassing our in vivo imaging region (200 μm within pia surface), approximately 98% of tdTomato-positive cells coexpressed the astrocytic marker S100β and 90% of S100β-labeled cells were tdTomato positive. In contrast, less than 1% of neurons (NeuN-positive), oligodendrocytes (Olig2-positive), and microglia (Iba1-positive) were tdTomato positive (Figure 1C). In deeper cortical layers, some of the S100β-positive cells failed to be labeled by the reporter, resulting in 75% of S100β-positive cells that are tdTomato-positive across all cortical layers (Supplemental Figure S1). These results suggest that Cre-mediated recombination occurs selectively and efficiently in cortical astrocytes.

In order to examine FMRP expression in astrocytes, we cultured cortical astrocytes from P4–5 mice of all genotypes (22). Immunocytochemistry revealed that all cultured cells expressed the astrocyte-specific markers S100β and ALDH1L1 (Figure 1D), and FMRP was absent from the cytoplasm of cultured astrocytes derived from *Fmr1*$^{fl/y}$*; mGFAP-Cre*$^{+}$ mice, but abundant in the cytoplasm of astrocytes from *Fmr1*$^{fl/y}$ mice (Figure 1E). Moreover, FMRP was not detectable by Western blot in lysates of cultured astrocytes derived from *Fmr1*$^{fl/y}$*;mGFAP-Cre*$^{+}$ mice (Figure 1F).

Because cultured astrocytes may not reflect their in vivo state, we sought to directly examine *Fmr1* expression in vivo. Unfortunately, because of the inherently low FMRP levels in astrocytes compared with neurons (19), in situ FMRP examination by standard immunohistochemical staining is not feasible. Therefore, we measured *Fmr1* mRNA transcript levels in astrocytes isolated acutely from adolescent mice (P30–50). To do so, we crossed *Fmr1*$^{fl/y}$ and *Fmr1*$^{fl/y}$*; mGFAP-Cre*$^{+}$ mice with *S100β-GFP* mice [a mouse line that selectively expresses GFP in astrocytes (35)] and isolated GFP-positive cells using fluorescence activated cell sorting (23,24). We found that sorted cells were enriched for the astrocytic marker *Aqp4*, but did not express the neuronal marker *Syt1* or the oligodendrocyte marker *Mog* (Figure 1G). Importantly, reverse-transcriptase polymerase chain reaction examination revealed that astrocytes sorted from *Fmr1*$^{fl/y}$*; mGFAP-Cre*$^{+}$*;S100β-GFP* mice did not express *Fmr1* mRNA (Figure 1H), in contrast to astrocytes sorted from *Fmr1*$^{+/y}$*; S100β-GFP* and *Fmr1*$^{fl/y}$*;S100β-GFP* mice. These results corroborate our findings in cultured astrocytes and provide in vivo proof that FMRP expression is selectively abolished in cortical astrocytes of *Fmr1*$^{fl/y}$*; mGFAP-Cre*$^{+}$ mice.

Next, we examined neuronal FMRP expression of astrocyte-specific *Fmr1* KO mice by immunohistochemistry. We found that nearly all (99.9%) NeuN-labeled cells coexpressed FMRP in the cortex of *Fmr1*$^{+/y}$, *Fmr1*$^{fl/y}$, and *Fmr1*$^{fl/y}$*; mGFAP-Cre*$^{+}$ mice, whereas no FMRP signal was detected in *Fmr1*$^{-/y}$ cortices (Figure 2A, B). Integrated density measurements of FMRP immunofluorescent signal within NeuN-labeled cells showed that neuronal FMRP levels were normal in *Fmr1*$^{fl/y}$*;mGFAP-Cre*$^{+}$ mice (Figure 2A, C). These results confirm that mGFAP-Cre–mediated recombination did not perturb FMRP expression in cortical neurons of *Fmr1*$^{fl/y}$*; mGFAP-Cre*$^{+}$ mice. Finally, we asked if the loss of FMRP induces gross abnormalities in cortical astrocytes. To do so, we immunostained astrocytes with S100β and conducted

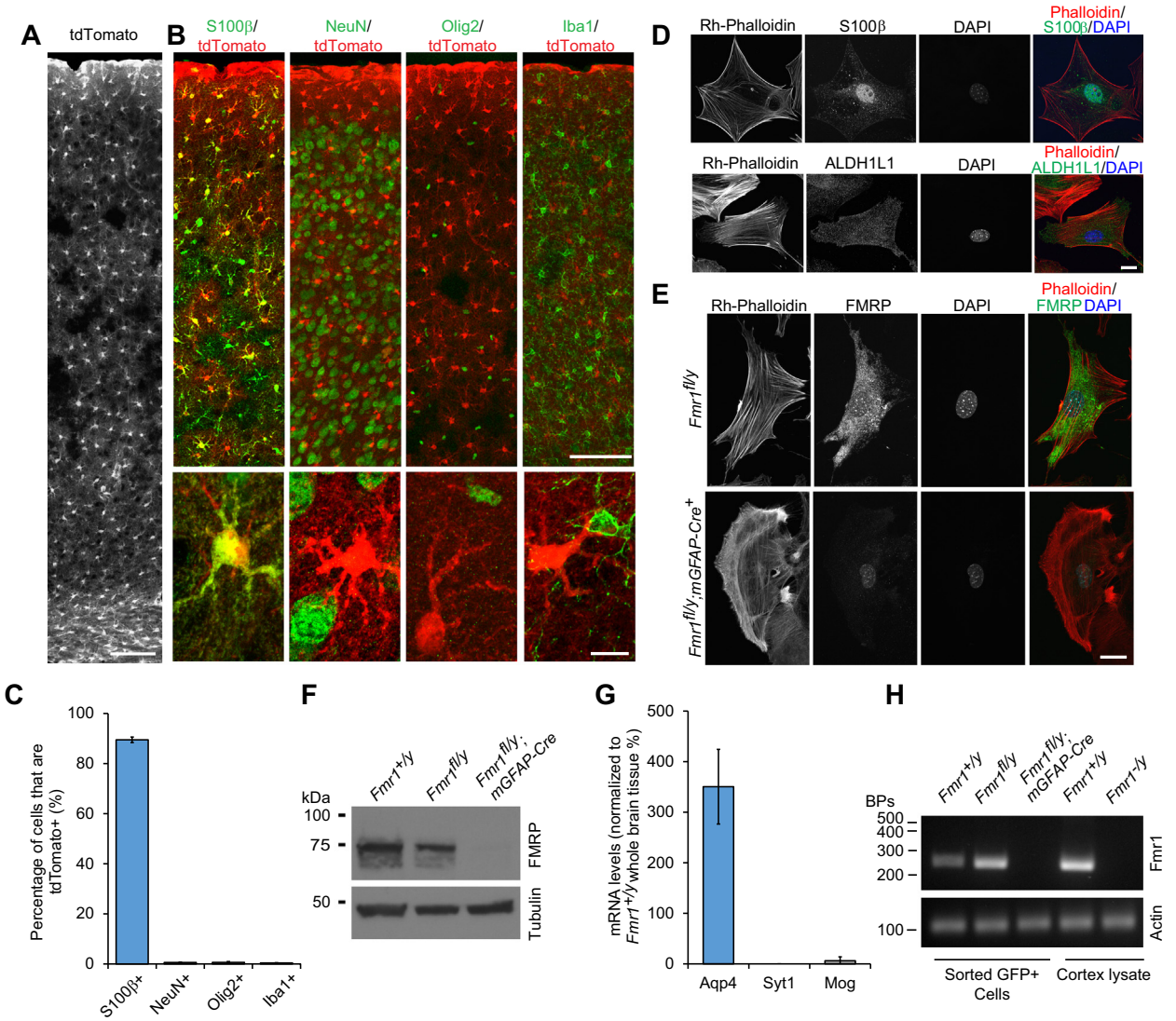

Figure 1. Fragile X mental retardation protein (FMRP) expression is abolished in astrocytes of astrocyte-specific *Fmr1* knockout mice. **(A)** A coronal section of the motor cortex from an *mGFAP-Cre*$^{+}$;*R26*^{tdTomato} mouse shows the distribution of cells targeted by mouse astrocytic glial fibrillary acidic protein (mGFAP-Cre)-mediated recombination. Scale bar = 100 μm. **(B)** Confocal images (low and high magnification) of immunolabeling for S100β, NeuN, Olig2, and Iba1 in *mGFAP-Cre*$^{+}$;*R26*^{tdTomato} mice show that tdTomato-positive cells coexpress the astrocytic marker S100β, but not the neuronal marker NeuN, the oligodendrocyte label Olig2, or the microglia marker Iba1 in the motor cortex. Scale bars = 100 μm (upper panel) and 10 μm (lower panel). **(C)** Quantitative analyses show the percentage of S100β-, NeuN-, Olig2-, and Iba1-immunolabeled cells colabeled with tdTomato-positive cells in the superficial motor cortex of *mGFAP-Cre*$^{+}$;*R26*^{tdTomato} mice. Data presented as mean ± SEM. **(D)** Cultured cortical astrocytes derived from postnatal day 4 to 5 *Fmr1*$^{fl/y}$ mice are immunoreactive for the astrocytic markers S100β and ALDH1L1. Rhodamine phalloidin was used to label F-actin. Scale bar = 25 μm. **(E)** Immunocytochemistry reveals a loss of FMRP in cultured cortical astrocytes derived from *Fmr1*$^{fl/y}$;*mGFAP-Cre*$^{+}$ mice. Scale bar = 25 μm. **(F)** Western blot on cultured astrocytes confirmed the absence of FMRP in astrocytes harvested from *Fmr1*$^{fl/y}$;*mGFAP-Cre*$^{+}$ mice. **(G)** Green fluorescent protein (GFP)-positive sorted cells are enriched for the astrocytic marker *Aqp4*, but lack the neuronal marker *Syt1* or the oligodendrocyte marker *Mog*. **(H)** Astrocytes sorted from adolescent *Fmr1*$^{fl/y}$;*mGFAP-Cre*$^{+}$;*S100β-GFP* mice do not express *Fmr1* messenger RNA (mRNA). Reverse-transcriptase polymerase chain reaction products on RNA extracted from cortical tissue of *Fmr1*$^{+/y}$ and *Fmr1*$^{-/y}$ mice serve as positive and negative controls, respectively.

stereological analysis. We found that the number and cell body volume of cortical astrocytes are comparable between *Fmr1*$^{+/y}$ and *Fmr1*$^{fl/y}$;*mGFAP-Cre*$^{+}$ mice (Figure 2D–F). Additionally, GFAP immunoreactivity was unaltered in the cortex of *Fmr1*$^{-/y}$ and *Fmr1*$^{fl/y}$;*mGFAP-Cre*$^{+}$ mice (data not shown), suggesting that the loss of FMRP does not induce reactive astrocytes.

Adult Astrocyte-Specific *Fmr1* KO Mice Have Impaired Motor Learning and Abundant Immature Dendritic Spines in the Motor Cortex

Patients with FXS have impaired learning and memory (3). A recent study also indicates that global *Fmr1* KO mice exhibit deficiencies in learning a skilled motor task (11). To ascertain

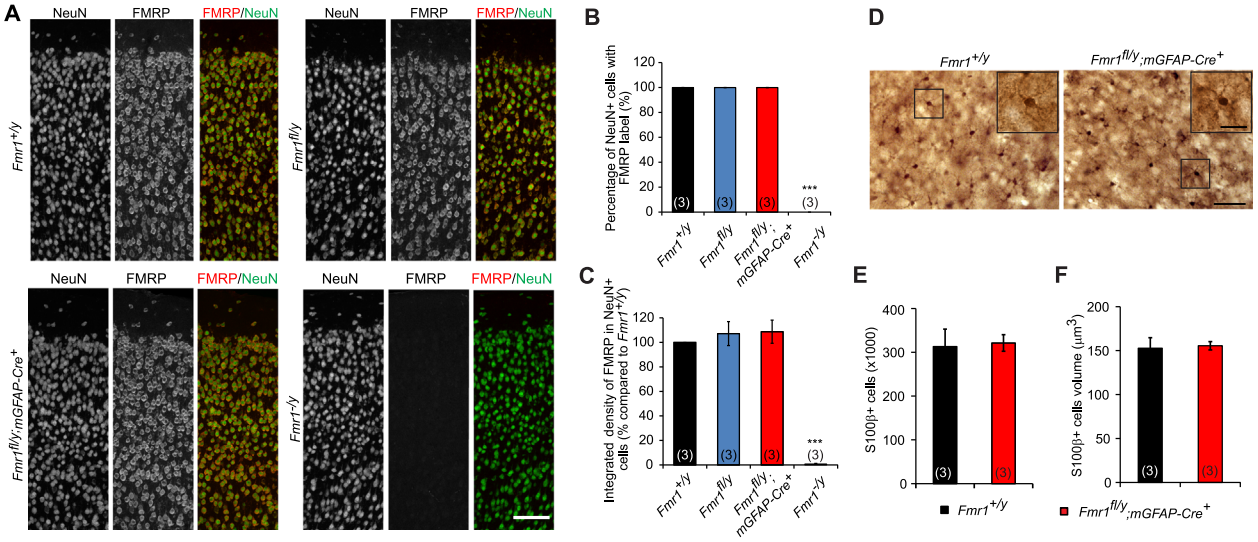

Figure 2. Neuronal fragile X mental retardation protein (FMRP) expression and gross astrocyte morphology are unperturbed in astrocyte-specific *Fmr1* knockout mice. **(A)** Confocal images of immunohistochemistry labeling for FMRP reveal normal neuronal FMRP expression in *Fmr1*$^{+/y}$, *Fmr1*$^{fl/y}$, and *Fmr1*$^{fl/y}$;*mGFAP-Cre*$^{+}$ mice, but none in *Fmr1*$^{-/y}$ mice. Scale bar = 100 μm. **(B)** In all genotypes except *Fmr1*$^{-/y}$ mice, 99.9% of the NeuN-positive cells coexpressed FMRP in coronal sections of the motor cortex. **(C)** The integrated densities of FMRP immunofluorescence within NeuN-labeled cells in the motor cortex are equivalent among *Fmr1*$^{+/y}$, *Fmr1*$^{fl/y}$, and *Fmr1*$^{fl/y}$;*mGFAP-Cre*$^{+}$ mice, but absent in *Fmr1*$^{-/y}$ mice. **(D)** Bright-field images of S100β immunolabeling in the cortex of *Fmr1*$^{+/y}$ and *Fmr1*$^{fl/y}$;*mGFAP-Cre*$^{+}$ mice. Scale bar = 50 μm. Inserts show individual astrocytes from boxed regions. Scale bar = 20 μm. **(E, F)** Quantification of cell number **(E)** and cell body volume **(F)** of cortical astrocytes reveal no significant difference between *Fmr1*$^{+/y}$ and *Fmr1*$^{fl/y}$;*mGFAP-Cre*$^{+}$ mice. ***$p < .001$. p values represent a comparison to *Fmr1*$^{+/y}$ mice. Numbers of mice analyzed are indicated in the figure.

whether *Fmr1*$^{fl/y}$;*mGFAP-Cre*$^{+}$ mice are also impaired in motor-skill learning, we trained mice with the single-pellet reaching task (25,30). We found that success rates on the first day of training were comparable among adult (>4 months old) *Fmr1*$^{+/y}$, *Fmr1*$^{fl/y}$, *Fmr1*$^{fl/y}$;*mGFAP-Cre*$^{+}$, and *Fmr1*$^{-/y}$ mice. Although *Fmr1*$^{+/y}$ and *Fmr1*$^{fl/y}$ mice improved their motor performance over time, *Fmr1*$^{fl/y}$;*mGFAP-Cre*$^{+}$ and *Fmr1*$^{-/y}$ mice failed to do so (Figure 3A). Therefore, *Fmr1* deletion in astrocytes alone suffices to impair motor-skill learning.

In vivo imaging studies have shown that baseline spine dynamics predict song learning capability in birds (36), and spine dynamics in the rodent motor cortex directly correlate with learning outcome (25). Therefore, we investigated spine dynamics in the motor cortex of FMRP-deficient mice. To visualize dendritic spines in vivo, we bred mice of all genotypes with YFP-H line mice, which express cytoplasmic yellow fluorescent protein (YFP) in a subset of cortical layer V pyramidal neurons (37). We found that baseline rates of spine formation and elimination along apical dendrites of layer V pyramidal neurons in the motor cortex were comparable among adult *Fmr1*$^{+/y}$, *Fmr1*$^{fl/y}$, *Fmr1*$^{fl/y}$;*mGFAP-Cre*$^{+}$, and *Fmr1*$^{-/y}$ mice prior to motor-skill training (Figure 3B, C). However, continuous motor training failed to increase spine dynamics in adult *Fmr1*$^{fl/y}$;*mGFAP-Cre*$^{+}$ mice (Figure 3B, C), which coincided with little improvement of their motor skill performance during training. Moreover, both *Fmr1*$^{fl/y}$;*mGFAP-Cre*$^{+}$ and *Fmr1*$^{-/y}$ mice displayed significantly higher spine densities than *Fmr1*$^{+/y}$ and *Fmr1*$^{fl/y}$ mice in adulthood (Figure 3D, E). Specifically, the density of morphologically immature thin spines was greatly elevated in *Fmr1*$^{fl/y}$;*mGFAP-Cre*$^{+}$ and *Fmr1*$^{-/y}$ mice, whereas the densities of other spine types were unchanged (Figure 3F). Additional analysis revealed that although spine head diameters were comparable among *Fmr1*$^{+/y}$, *Fmr1*$^{fl/y}$, *Fmr1*$^{fl/y}$;*mGFAP-Cre*$^{+}$, and *Fmr1*$^{-/y}$ mice, spine neck lengths in *Fmr1*$^{-/y}$ and *Fmr1*$^{fl/y}$;*mGFAP-Cre*$^{+}$ mice were significantly longer than those in *Fmr1*$^{+/y}$ and *Fmr1*$^{fl/y}$ mice (Supplemental Figure S2). It is worth noting that the spine density observed in *Fmr1*$^{-/y}$ mice was significantly higher than that in *Fmr1*$^{fl/y}$;*mGFAP-Cre*$^{+}$ mice, implying that the global loss of FMRP exacerbates the salient spine phenotype. These results reveal that silencing *Fmr1* selectively in astrocytes contributes to both synaptic and learning defects in adult mice.

Deletion of *Fmr1* in Astrocytes Heightens Spine Formation During Adolescent Development

Noting the resemblance of immature spines in patients with FXS to those observed during early development, researchers have hypothesized that *Fmr1* silencing leads to defects in spine pruning (i.e., net loss of spines) (14). Having shown that adult astrocyte-specific and global *Fmr1* KO mice exhibit significantly more immature spines, we next investigated whether this phenotype was due to defective spine pruning. We imaged spines in the motor cortex of adolescent mice between 4 and 6 weeks old, an age typically associated with a substantial reduction in spine number (29). We found that the density and morphology of dendritic spines were comparable among *Fmr1*$^{+/y}$, *Fmr1*$^{fl/y}$, *Fmr1*$^{fl/y}$;*mGFAP-Cre*$^{+}$, and *Fmr1*$^{-/y}$ mice at 1 month of age (Figure 4A). Coinciding with normal spine phenotypes, adolescent *Fmr1*$^{fl/y}$;*mGFAP-Cre*$^{+}$ and *Fmr1*$^{-/y}$ mice displayed normal motor learning when trained

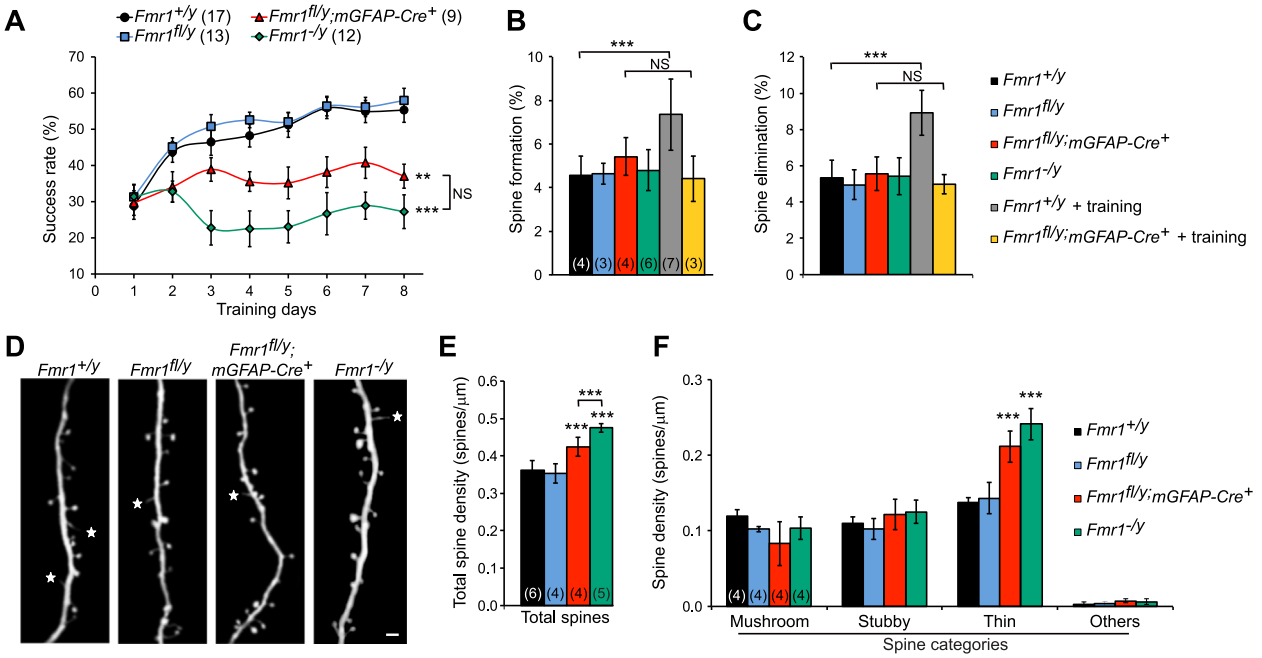

Figure 3. Deletion of *Fmr1* in astrocytes elevated spine density and impaired motor-skill learning in adult mice. **(A)** Adult *Fmr1*$^{fl/y}$*;mGFAP-Cre*$^{+}$ and *Fmr1*$^{-/y}$ mice fail to improve their success rates during training in single-pellet reaching tasks, whereas *Fmr1*$^{+/y}$ and *Fmr1*$^{fl/y}$ mice improve their performance. **(B, C)** Motor cortical spine formation **(B)** and elimination **(C)** over 4 days are normal in *Fmr1*$^{fl/y}$*;mGFAP-Cre*$^{+}$ and *Fmr1*$^{-/y}$ mice under baseline. Spine turnover increases in *Fmr1*$^{+/y}$ mice during motor training, but does not change significantly (NS) in *Fmr1*$^{fl/y}$*;mGFAP-Cre*$^{+}$ mice. **(D)** In vivo two-photon imaging shows spines and filopodia (asterisks) on dendritic segments of layer V neurons from adult *Fmr1*$^{+/y}$, *Fmr1*$^{fl/y}$, *Fmr1*$^{fl/y}$*;mGFAP-Cre*$^{+}$, and *Fmr1*$^{-/y}$ mice. Scale bar = 2 µm. **(E, F)** *Fmr1*$^{fl/y}$*;mGFAP-Cre*$^{+}$ and *Fmr1*$^{-/y}$ mice exhibit higher total spine density **(E)** and higher density of thin spines **(F)**. $^{**}p < .01$, $^{***}p < .001$. *p* values represent a comparison to *Fmr1*$^{+/y}$ mice unless otherwise indicated. Numbers of mice analyzed indicated in the figure.

with the single-pellet reaching task (Figure 4B). Surprisingly, the extent of baseline spine loss over various intervals (i.e., 1, 4, or 16 days) was also similar among *Fmr1*$^{+/y}$, *Fmr1*$^{fl/y}$, *Fmr1*$^{fl/y}$*;mGFAP-Cre*$^{+}$, and *Fmr1*$^{-/y}$ mice (Figure 4C, E). However, significantly more new spines were accumulated over 4 and 16 days in *Fmr1*$^{fl/y}$*;mGFAP-Cre*$^{+}$ and *Fmr1*$^{-/y}$ mice (Figure 4C, D). The disparity between the generation and removal of spines led to a net difference in total spine numbers on day 4, measured as a percentage of spine number on day 0 (Figure 4F). Dendrites in the developing mouse cortex also harbor filopodia. Filopodia are long thin protrusions without bulbuous heads; they are presumably the precursors of dendritic spines (38). We found that filopodia exhibited normal density, daily turnover, and conversion rate to spines (data not shown), indicating that excess spine accumulation is not due to overproduction or altered dynamics of filopodia. Together, our results suggest that selective silencing of *Fmr1* in astrocytes causes overproduction of spines during adolescence, which is not compensated by spine pruning. Furthermore, the abnormalities in adolescent spine dynamics precede behavioral impairments in adulthood.

Generation of Astrocyte-Specific *Fmr1* Rescue Mice

Selective astrocytic restoration of the Rett syndrome gene *Mecp2* in global MeCP2-deficient mice has been shown to significantly improve various behavioral and neuronal abnormalities associated with Rett syndrome (39). Therefore, we sought to determine whether exclusive FMRP expression in astrocytes alone could rescue defects in spine development and brain function. To do so, we crossed *mGFAP-Cre* mice with mice harboring an *Fmr1* gene in which a neomycin selection cassette is flanked by *loxP* sites in the first intron (*Fmr1*^{neo}) (34). Western blot and immunohistochemistry studies were performed to characterize neuronal and astrocytic FMRP expression in *Fmr1*$^{neo/y}$ and *Fmr1*$^{neo/y}$*;mGFAP-Cre*$^{+}$ mice. We found that perturbation of the *Fmr1* gene with a neomycin selection cassette (*Fmr1*$^{neo/y}$ mice) induced a dramatic reduction in total FMRP expression (17.7% of *Fmr1*$^{+/y}$ mice), but did not completely abolish *Fmr1* gene expression. Importantly, FMRP expression in the cortex of *Fmr1*$^{neo/y}$*;mGFAP-Cre*$^{+}$ mice was 122% greater than that of *Fmr1*$^{neo/y}$ mice (Figure 5A). This net increase in total cortical FMRP levels in *Fmr1*$^{neo/y}$*;mGFAP-Cre*$^{+}$ mice was specific to restoration of FMRP expression in astrocytes because mGFAP-Cre–mediated recombination increased astrocytic FMRP levels by about fourfold in comparison to *Fmr1*$^{neo/y}$ mice (Figure 5B). Furthermore, immunohistochemistry data revealed that neuronal FMRP expression in *Fmr1*$^{neo/y}$*;mGFAP-Cre*$^{+}$ mice was identical to that in *Fmr1*$^{neo/y}$ mice, with both genotypes showing 26.1% of the neuronal FMRP signal displayed by *Fmr1*$^{+/y}$ mice (Figure 5C, D). Overall, these results confirm that FMRP expression is selectively restored in astrocytes of *Fmr1*$^{neo/y}$*;mGFAP-Cre*$^{+}$ mice, whereas neuronal FMRP expression is significantly depressed in both genotypes.

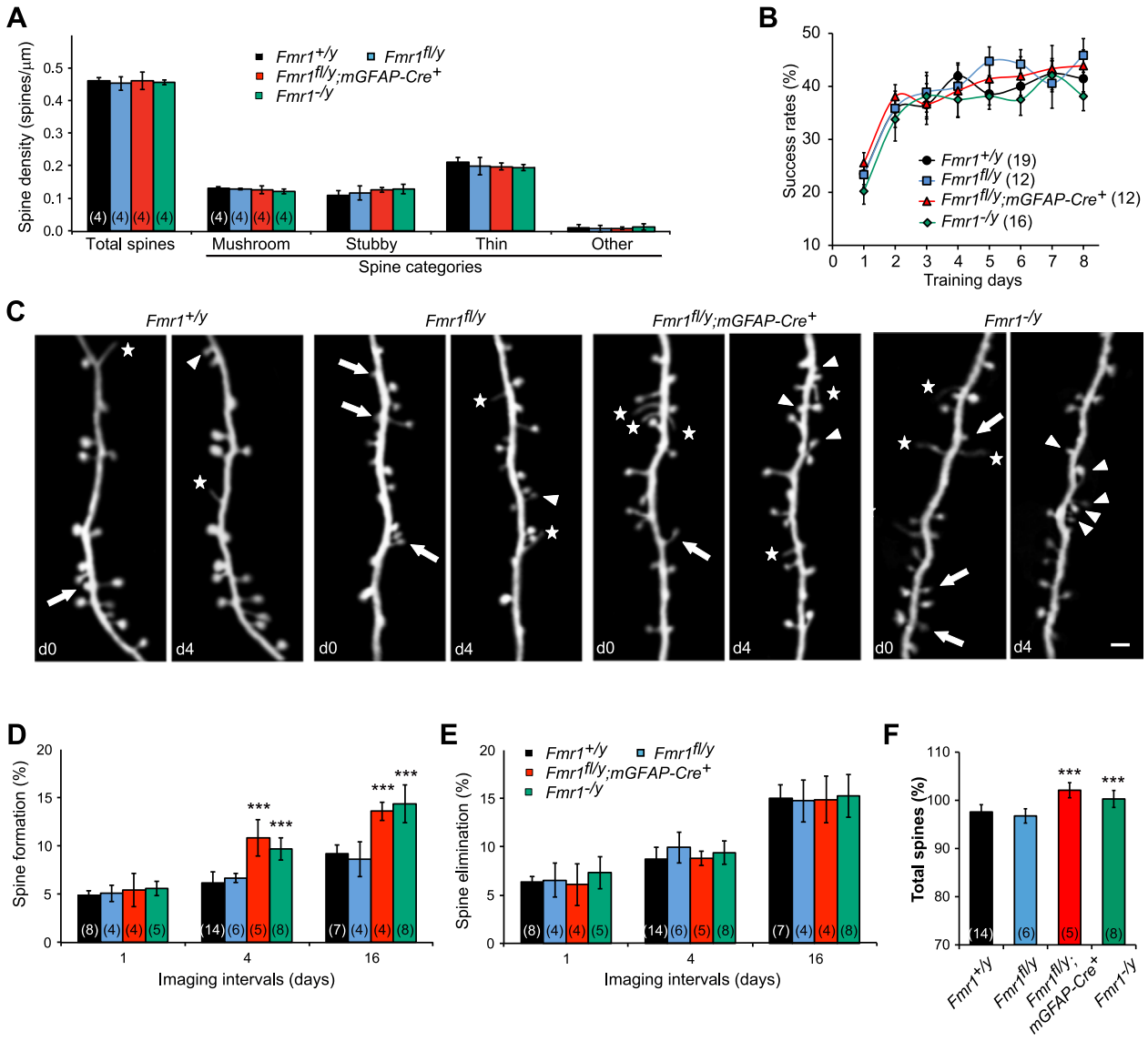

Figure 4. Spine formation is elevated in adolescent astrocyte-specific *Fmr1* knockout mice. **(A)** Spine density (total and in each of the four categories) is not significantly different between genotypes. **(B)** Adolescent mice of all genotypes improve their success rates over 8 days of training with the single-pellet reaching task. **(C)** Repeated imaging of the same dendritic branches over 4-day intervals in the motor cortex of 1-month-old *Fmr1*$^{+/y}$, *Fmr1*$^{fl/y}$, *Fmr1*$^{fl/y}$;*mGFAP-Cre*$^{+}$, and *Fmr1*$^{-/y}$ mice reveals newly formed spines (arrowheads), eliminated spines (arrows), and filopodia (asterisks). Scale bar = 2 µm. **(D, E)** *Fmr1*$^{fl/y}$;*mGFAP-Cre*$^{+}$ and *Fmr1*$^{-/y}$ mice exhibit elevated spine formation **(D)** albeit normal spine elimination **(E)** over 4- and 16-day intervals. **(F)** Compared with *Fmr1*$^{+/y}$ mice, the total number of spines on day 4 is higher in *Fmr1*$^{fl/y}$;*mGFAP-Cre*$^{+}$ and *Fmr1*$^{-/y}$ mice, but not in *Fmr1*$^{fl/y}$ mice (number of spines on day 0 = 100%). ***$p < .001$, p values represent a comparison to *Fmr1*$^{+/y}$ mice. Numbers of mice analyzed indicated in the figure. d, day.

Astrocytic FMRP Expression Alone Is Insufficient to Rescue Most of the Spine and Motor Learning Deficits

Despite low levels of neuronal and astrocytic FMRP expression in the brains of *Fmr1*$^{neo/y}$ mice, these mice displayed heightened spine formation during adolescence, recapitulating the spine phenotype observed in both global and astrocyte-specific *Fmr1* KO mice (Figures 4D, E, 6A, B). This suggests that global knock down of FMRP expression is sufficient to elicit FXS pathologies and that normal FMRP expression levels are required for proper brain function. However, re-expression of astrocytic FMRP in the *Fmr1*$^{neo/y}$ background did not correct the abnormal spine production in adolescence (Figure 6A, B). As a consequence, spine densities, particularly thin spine densities of adult *Fmr1*$^{neo/y}$;*mGFAP-Cre*$^{+}$ and *Fmr1*$^{neo/y}$ mice, were significantly higher than that of adult *Fmr1*$^{+/y}$ mice (Figure 6C, D). Intriguingly, although *Fmr1*$^{neo/y}$ mice exhibited comparable spine neck lengths as *Fmr1*$^{-/y}$ mice, *Fmr1*$^{neo/y}$;*mGFAP-Cre*$^{+}$ mice had a spine neck length distribution comparable to that of *Fmr1*$^{+/y}$ mice (Supplemental Figure S2B). Additionally, both *Fmr1*$^{neo/y}$ and *Fmr1*$^{neo/y}$;*mGFAP-Cre*$^{+}$ mice displayed defective motor-skill learning in

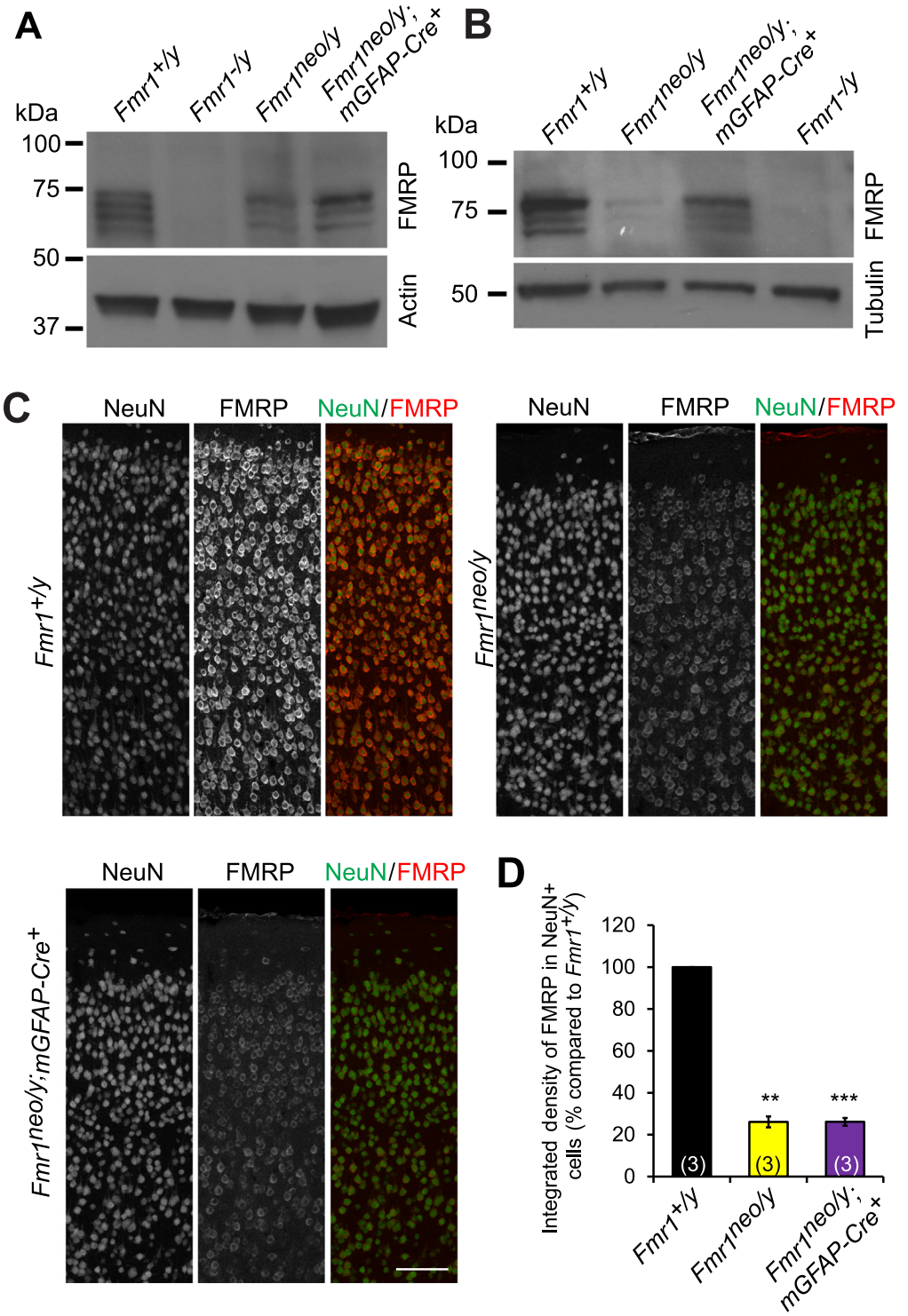

Figure 5. Fragile X mental retardation protein (FMRP) expression is selectively restored in astrocytes of *Fmr1*$^{neo/y}$;*mGFAP-Cre*$^{+}$ mice. **(A)** Western blot on cortex indicates that total cortical FMRP levels are higher in *Fmr1*$^{neo/y}$;*mGFAP-Cre*$^{+}$ mice than in *Fmr1*$^{neo/y}$ mice. **(B)** Western blot on cortical astrocytes shows that FMRP is expressed in *Fmr1*$^{neo/y}$;*mGFAP-Cre*$^{+}$ mice, but nearly absent in astrocytes from *Fmr1*$^{neo/y}$ mice. **(C)** Confocal images of immunohistochemistry labeling for FMRP and NeuN in the motor cortex reveal FMRP expression is dramatically reduced in cortical neurons of *Fmr1*$^{neo/y}$ and *Fmr1*$^{neo/y}$;*mGFAP-Cre*$^{+}$ mice compared with *Fmr1*$^{+/y}$ mice. Scale bar = 100 μm. **(D)** Quantification of the integrated density of FMRP immunofluorescent signal within NeuN-labeled cells in the motor cortex shows that neuronal FMRP levels are identical between *Fmr1*$^{neo/y}$ and *Fmr1*$^{neo/y}$;*mGFAP-Cre*$^{+}$ mice (both constituting 26.1% of neuronal FMRP signal in *Fmr1*$^{+/y}$ mice). $^{**}p < .005$, $^{***}p < .001$. *p* values represent a comparison to *Fmr1*$^{+/y}$ mice. Numbers of mice analyzed indicated in the figure.

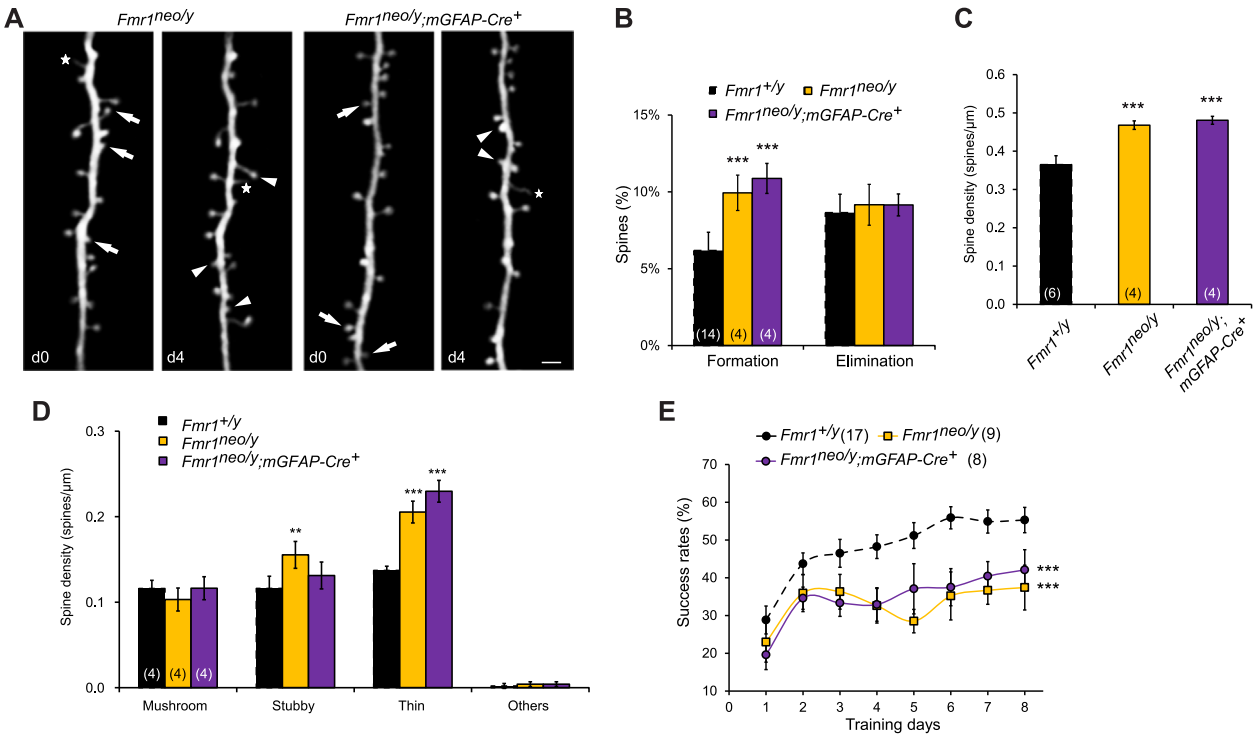

Figure 6. Restoration of astrocytic fragile X mental retardation protein (FMRP) in an *Fmr1* null background is insufficient to restore normal spine or motor-skill learning phenotypes. **(A)** Repeated imaging of the same dendritic branches over 4-day intervals in the motor cortex of 1-month-old *Fmr1*$^{neo/y}$ and *Fmr1*$^{neo/y}$*;mGFAP-Cre*$^{+}$ mice reveals newly formed spines (arrowheads), eliminated spines (arrows), and filopodia (asterisks). Scale bar = 2 µm. **(B)** *Fmr1*$^{neo/y}$ and *Fmr1*$^{neo/y}$*;mGFAP-Cre*$^{+}$ mice exhibit elevated spine formation albeit normal spine elimination over 4 days during adolescence. **(C, D)** Adult *Fmr1*$^{neo/y}$ and *Fmr1*$^{neo/y}$*;mGFAP-Cre*$^{+}$ mice display a higher total spine density (**C**) and a greater density of thin spines **(D). (E)** Adult *Fmr1*$^{neo/y}$ and *Fmr1*$^{neo/y}$*;mGFAP-Cre*$^{+}$ mice fail to improve their success rates during training with the single-pellet reaching task. $^{**}p < .01$, $^{***}p < .001$. *p* values represent a comparison to *Fmr1*$^{+/y}$ mice. Numbers of mice analyzed indicated in the figure. d, day.

adulthood (Figure 6E). Together, these data suggest that *Fmr1* expression in nonastrocytic cells (e.g., neurons and possibly other cell types) is also required for normal spine dynamics and motor learning.

DISCUSSION

Our study, for the first time, reveals in vivo the contribution of astrocytes to the development of spine abnormalities and behavioral defects in FXS. We showed that loss of FMRP in astrocytes leads to increases in spine production along apical dendrites of layer V pyramidal neurons in the motor cortex of adolescent mice. This increase in spine formation occurs at a time when neuronal circuits in the motor cortex are normally being refined through the pruning of synaptic connections and results in supernumerary morphologically immature spines in adulthood. Furthermore, motor-skill training failed to promote spine turnover in the motor cortex of astrocyte-specific *Fmr1* KO mice, paralleling the animal's inability to learn the motor task during adulthood.

In response to several neurodevelopmental and neurodegenerative diseases, as well as central nervous system injury, astrocytes are known to undergo morphological alterations, including hypertrophy of the cell body and processes (17,40). However, in vivo data for astrocyte morphology in FXS are few and inconsistent. One group reports no astrogliosis seen in postmortem brains of persons with FXS (41). However, an elevated number of activated astrocytes was observed in the cerebellum of *Fmr1* KO mice (42). Our results show no gross changes in volume or reactivity of cortical astrocytes, but we cannot exclude that subtle changes to the fine astrocyte processes or alterations in astrocytic signaling exist.

The overabundance of immature spines found in the cortex of both adult *Fmr1* KO mice and human patients with FXS has traditionally been attributed to a defect in spine pruning (14). Our longitudinal in vivo imaging results show that heightened spine density in adult global and astrocyte-specific FMRP-deficient mice is likely a consequence of accumulation of spines generated during adolescence. Furthermore, the increase in adult spine density is attributable to the overabundance of thin spines, for which the morphology resembles that of immature spines lacking functional synapses (43). In hippocampal neurons cultured from *Fmr1* KO mice, significantly fewer spines are juxtaposed to presynaptic terminals (44). Attenuated connectivity, despite an overabundance of spines, may explain why neuronal circuits associated with motor learning do not function appropriately in FXS. Our work demonstrates that normal FMRP expression is indispensable in both neurons and astrocytes because restoration of FMRP expression in astrocytes alone failed to completely ameliorate the aberrant spine pathology and behavioral abnormalities

associated with FXS. Interestingly, loss of FMRP expression in either astrocytes alone or in all brain cells except the astrocytes engendered nearly identical spine and behavior phenotypes. This raises the intriguing notion that FMRP functions in a non–cell-autonomous manner to indirectly regulate spine dynamics by pathways paramount to neuron-glia communication.

Several molecules involved in regulating neuron-glia interactions have been implicated in FXS, including the major glutamate transporter GLT-1 (19), matrix metalloproteinase 9 (MMP-9) (45), and the astrocytic-secreted growth factor neurotrophin-3 (46). Loss of function or overexpression of these molecules has been shown to affect spine pathology. A recent study showed that *Fmr1* deletion in astrocytes in vivo reduced expression of the major glutamate transporter GLT-1, which normally functions to control extracellular synaptic glutamate levels (47). Loss of GLT-1–mediated glutamate uptake elevated the level of extracellular glutamate and consequently increased the excitability of layer V pyramidal neurons (19,47). Because an increased local glutamate concentration may promote de novo spine growth (48), dysregulated glutamate homeostasis induced by the loss of FMRP in astrocytes may partially account for the increased spine formation observed in global and astrocyte-specific *Fmr1* KO mice.

In addition, transgenic animals overexpressing MMP-9 display an increased density of immature spines and impaired social interaction similar to that of *Fmr1* KO mice (45,49). Translation of MMP-9 mRNA at the synapse is normally repressed by FMRP (50). Because MMP-9 is secreted by both neurons and glia (51), it is possible that excessive amounts of MMP-9 are produced at the synaptic cleft, resulting in erroneous spine formation regardless of whether FMRP is absent in either neurons or astrocytes. The mechanisms by which astrocytic FMRP regulates astrocyte signaling and alters neuron-glia interactions remains unknown. Future molecular dissection of the function of FMRP in astrocytes, as well as the uncovering of mRNAs that FMRP translationally controls in astrocytes, will reveal its role in astrocytic regulation of spine dynamics and shed new light on FXS etiology.

ACKNOWLEDGMENTS AND DISCLOSURES

This work was supported by grants from the National Institute of Mental Health (Grant Nos. R01MH104227 and R01MH094449 to YZ) and National Institute of Neurological Disorders and Stroke (Grant No. R01NS078791 to YZ).

We thank Drs. David L. Nelson, Stephen T. Warren, Michael V. Sofroniew, and Wesley J. Thompson for providing mouse lines used in this study; Benjamin Abrams (University of California, Santa Cruz, Life Sciences Microscopy Center), Bari Holm Nazario (Manager of the Institute for the Biology of Stem Cells Flow Cytometry Facility), Lavpreet Jammu, Sabyn Nopar, and Audrey Re for assistance with experiments; Caitlin Moyer for critical comments on the manuscript; Ben Barres' laboratory (Stanford) for helpful advice regarding immunopanning experiments and sharing hybridoma supernatants; and Camilla Forsberg's laboratory (University of California, Santa Cruz) and Blanca Diaz Castro (University of California, Los Angeles) for advice regarding fluorescence-activated cell sorting and reverse-transcriptase polymerase chain reaction.

The authors report no biomedical financial interests or potential conflicts of interest.

ARTICLE INFORMATION

From the Department of Molecular, Cell and Developmental Biology (JLH, XY, AG, HB, MT, JFP, C-CC, JL, YZ), University of California Santa Cruz, Santa Cruz, California; and The Brain Cognition and Brain Disease Institute (XL), Shenzhen Institutes of Advanced Technology, Chinese Academy of Sciences, Shenzhen, China.

JLH and XY contributed equally to this work.

Address correspondence to Yi Zuo, Ph.D., Department of Molecular, Cell and Developmental Biology, University of California Santa Cruz, 1156 High Street, Santa Cruz, CA 95064; E-mail: yizuo@ucsc.edu.

Received May 4, 2016; revised Aug 12, 2016; accepted Aug 30, 2016.

Supplementary material cited in this article is available online at http://dx.doi.org/10.1016/j.biopsych.2016.08.036.

REFERENCES

1. Warren ST, Nelson DL (1994): Advances in molecular analysis of fragile X syndrome. JAMA 271:536–542.
2. Penagarikano O, Mulle JG, Warren ST (2007): The pathophysiology of fragile x syndrome. Annu Rev Genom Hum Genet 8:109–129.
3. Fisch GS, Simensen RJ, Schroer RJ (2002): Longitudinal changes in cognitive and adaptive behavior scores in children and adolescents with the fragile X mutation or autism. J Autism Dev Disord 32: 107–114.
4. Berry-Kravis E (2002): Epilepsy in fragile X syndrome. Dev Med Child Neurol 44:724–728.
5. Pieretti M, Zhang FP, Fu YH, Warren ST, Oostra BA, Caskey CT, *et al*. (1991): Absence of expression of the FMR-1 gene in fragile X syndrome. Cell 66:817–822.
6. Bassell GJ, Warren ST (2008): Fragile X syndrome: Loss of local mRNA regulation alters synaptic development and function. Neuron 60:201–214.
7. Holtmaat A, Svoboda K (2009): Experience-dependent structural synaptic plasticity in the mammalian brain. Nat Rev Neurosci 10: 647–658.
8. Nimchinsky EA, Sabatini BL, Svoboda K (2002): Structure and function of dendritic spines. Annu RevPhysiol 64:313–353.
9. Pan F, Aldridge GM, Greenough WT, Gan WB (2010): Dendritic spine instability and insensitivity to modulation by sensory experience in a mouse model of fragile X syndrome. Proc Natl Acad Sci U S A 107: 17768–17773.
10. Cruz-Martin A, Crespo M, Portera-Cailliau C (2010): Delayed stabilization of dendritic spines in fragile X mice. J Neurosci 30: 7793–7803.
11. Padmashri R, Reiner BC, Suresh A, Spartz E, Dunaevsky A (2013): Altered structural and functional synaptic plasticity with motor skill learning in a mouse model of fragile X syndrome. J Neurosci 33: 19715–19723.
12. Hinton VJ, Brown WT, Wisniewski K, Rudelli RD (1991): Analysis of neocortex in three males with the fragile X syndrome. Am J Med Genet 41:289–294.
13. Comery TA, Harris JB, Willems PJ, Oostra BA, Irwin SA, Weiler IJ, *et al*. (1997): Abnormal dendritic spines in fragile X knockout mice: maturation and pruning deficits. Proc Natl Acad Sci U S A 94: 5401–5404.
14. Bagni C, Greenough WT (2005): From mRNP trafficking to spine dysmorphogenesis: the roots of fragile X syndrome. Nat Rev Neurosci 6:376–387.
15. Dailey ME, Smith SJ (1996): The dynamics of dendritic structure in developing hippocampal slices. J Neurosci 16:2983–2994.
16. Bear MF, Huber KM, Warren ST (2004): The mGluR theory of fragile X mental retardation. Trends Neurosci 27:370–377.
17. Molofsky AV, Krencik R, Ullian EM, Tsai HH, Deneen B, Richardson WD, *et al*. (2012): Astrocytes and disease: A neurodevelopmental perspective. Genes Dev 26:891–907.
18. Pacey LK, Doering LC (2007): Developmental expression of FMRP in the astrocyte lineage: Implications for fragile X syndrome. Glia 55: 1601–1609.

19. Higashimori H, Morel L, Huth J, Lindemann L, Dulla C, Taylor A, *et al*. (2013): Astroglial FMRP-dependent translational down-regulation of mGluR5 underlies glutamate transporter GLT1 dysregulation in the fragile X mouse. Hum Mol Genet 22:2041–2054.
20. Gholizadeh S, Halder SK, Hampson DR (2015): Expression of fragile X mental retardation protein in neurons and glia of the developing and adult mouse brain. Brain Res 1596:22–30.
21. Jacobs S, Doering LC (2010): Astrocytes prevent abnormal neuronal development in the fragile x mouse. J Neurosci 30:4508–4514.
22. Schildge S, Bohrer C, Beck K, Schachtrup C (2013): Isolation and culture of mouse cortical astrocytes. J Vis Exp Jan 19;(71).
23. Cahoy JD, Emery B, Kaushal A, Foo LC, Zamanian JL, Christopherson KS, *et al*. (2008): A transcriptome database for astrocytes, neurons, and oligodendrocytes: A new resource for understanding brain development and function. J Neurosci 28:264–278.
24. Foo LC (2013): Purification of rat and mouse astrocytes by immunopanning. Cold Spring Harbor Protocols 2013:421–432.
25. Xu T, Yu X, Perlik AJ, Tobin WF, Zweig JA, Tennant K, *et al*. (2009): Rapid formation and selective stabilization of synapses for enduring motor memories. Nature 462:915–919.
26. Yu X, Zuo Y (2014): Two-photon in vivo imaging of dendritic spines in the mouse cortex using a thinned-skull preparation. J Vis Exp May 12;(87).
27. Harris KM, Jensen FE, Tsao B (1992): Three-dimensional structure of dendritic spines and synapses in rat hippocampus (CA1) at postnatal day 15 and adult ages: Implications for the maturation of synaptic physiology and long-term potentiation. J Neurosci 12:2685–2705.
28. Araya R, Vogels TP, Yuste R (2014): Activity-dependent dendritic spine neck changes are correlated with synaptic strength. Proc Natl Acad Sci United States of America 111:E2895–2904.
29. Zuo Y, Lin A, Chang P, Gan WB (2005): Development of long-term dendritic spine stability in diverse regions of cerebral cortex. Neuron 46:181–189.
30. Chen CC, Gilmore A, Zuo Y (2014): Study motor skill learning by single-pellet reaching tasks in mice. J Vis Exp Mar 4;(85).
31. Garcia AD, Doan NB, Imura T, Bush TG, Sofroniew MV (2004): GFAP-expressing progenitors are the principal source of constitutive neurogenesis in adult mouse forebrain. Nat Neurosci 7:1233–1241.
32. Imura T, Kornblum HI, Sofroniew MV (2003): The predominant neural stem cell isolated from postnatal and adult forebrain but not early embryonic forebrain expresses GFAP. J Neurosci 23:2824–2832.
33. Tao J, Wu H, Lin Q, Wei W, Lu XH, Cantle JP, *et al*. (2011): Deletion of astroglial Dicer causes non-cell-autonomous neuronal dysfunction and degeneration. J Neurosci 31:8306–8319.
34. Mientjes EJ, Nieuwenhuizen I, Kirkpatrick L, Zu T, Hoogeveen-Westerveld M, Severijnen L, *et al*. (2006): The generation of a conditional Fmr1 knock out mouse model to study Fmrp function in vivo. Neurobiol Dis 21:549–555.
35. Zuo Y, Lubischer JL, Kang H, Tian L, Mikesh M, Marks A, *et al*. (2004): Fluorescent proteins expressed in mouse transgenic lines mark subsets of glia, neurons, macrophages, and dendritic cells for vital examination. J Neurosci 24:10999–11009.
36. Roberts TF, Tschida KA, Klein ME, Mooney R (2010): Rapid spine stabilization and synaptic enhancement at the onset of behavioural learning. Nature 463:948–952.
37. Feng G, Mellor RH, Bernstein M, Keller-Peck C, Nguyen QT, Wallace M, *et al*. (2000): Imaging neuronal subsets in transgenic mice expressing multiple spectral variants of GFP. Neuron 28:41–51.
38. Ziv NE, Smith SJ (1996): Evidence for a role of dendritic filopodia in synaptogenesis and spine formation. Neuron 17:91–102.
39. Lioy DT, Garg SK, Monaghan CE, Raber J, Foust KD, Kaspar BK, *et al*. (2011): A role for glia in the progression of Rett's syndrome. Nature 475:497–500.
40. Sun D, Jakobs TC (2012): Structural remodeling of astrocytes in the injured CNS. Neuroscientist 18:567–588.
41. Reiss AL, Aylward E, Freund LS, Joshi PK, Bryan RN (1991): Neuroanatomy of fragile X syndrome: the posterior fossa. Ann Neurol 29: 26–32.
42. Pacey LK, Guan S, Tharmalingam S, Thomsen C, Hampson DR (2015): Persistent astrocyte activation in the fragile X mouse cerebellum. Brain Behav 5:e00400.
43. Knott GW, Holtmaat A, Wilbrecht L, Welker E, Svoboda K (2006): Spine growth precedes synapse formation in the adult neocortex in vivo. Nat Neurosci 9:1117–1124.
44. Braun K, Segal M (2000): FMRP involvement in formation of synapses among cultured hippocampal neurons. Cereb Cortex 10:1045–1052.
45. Michaluk P, Wawrzyniak M, Alot P, Szczot M, Wyrembek P, Mercik K, *et al*. (2011): Influence of matrix metalloproteinase MMP-9 on dendritic spine morphology. J Cell Sci 124:3369–3380.
46. Yang Q, Feng B, Zhang K, Guo YY, Liu SB, Wu YM, *et al*. (2012): Excessive astrocyte-derived neurotrophin-3 contributes to the abnormal neuronal dendritic development in a mouse model of fragile X syndrome. PLoS Genet 8:e1003172.
47. Higashimori H, Schin CS, Chiang MS, Morel L, Shoneye TA, Nelson DL, *et al*. (2016): Selective deletion of astroglial FMRP dysregulates glutamate transporter GLT1 and contributes to fragile X syndrome phenotypes in vivo. J Neurosci 36:7079–7094.
48. Kwon HB, Sabatini BL (2011): Glutamate induces de novo growth of functional spines in developing cortex. Nature 474:100–104.
49. Gkogkas CG, Khoutorsky A, Cao R, Jafarnejad SM, Prager-Khoutorsky M, Giannakas N, *et al*. (2014): Pharmacogenetic inhibition of eIF4E-dependent Mmp9 mRNA translation reverses fragile X syndrome-like phenotypes. Cell Rep 9:1742–1755.
50. Janusz A, Milek J, Perycz M, Pacini L, Bagni C, Kaczmarek L, *et al*. (2013): The fragile X mental retardation protein regulates matrix metalloproteinase 9 mRNA at synapses. J Neurosci 33:18234–18241.
51. Huntley GW (2012): Synaptic circuit remodelling by matrix metalloproteinases in health and disease. Nat Rev Neurosci 13: 743–757.